

Accessing different higher-order modes with beam self-cleaning under simple realistic tuning of initial conditions

JULIEN DECHANXHE, PASCAL KOCKAERT, AND SPENCER W. JOLLY*

Service OPERA-Photonique, Université libre de Bruxelles (ULB), Brussels, Belgium

*spencer.jolly@ulb.be

Abstract: The initial conditions in multimode fibers pumped by ultrashort laser pulses strongly determine the following nonlinear optical interactions. In this work we firstly compare the detailed spatial mode content of simple initial conditions, transverse offset and tilt. We then show how those initial conditions can both be used to achieve beam self-cleaning into higher-order spatial modes of a model graded-index fiber, with their own slight differences and advantages. Going beyond purely spatial initial conditions, we introduce self-cleaning results using spatial chirp at the input facet, whereby the different temporal envelopes of the spatial modes allows for tuning the self-cleaning process. Our results open up investigations into higher-dimensional tuning of nonlinear processes in multimode fibers using initial conditions.

1. Introduction

Multimode fibers, optical fibers that are larger in core diameter and therefore admit more than one and sometimes a large number of propagating modes, have long been imagined as platforms for high-power lasers due the possibility of larger guided profiles. However, small perturbations in the fiber or weak interactions between modes can readily cause a degradation of mode quality, hence making the application to high-power lasers or typical telecommunications devices difficult. The complexities and high spatially frequency content of the linear propagation has however been utilized for enhanced imaging through multimode fiber endoscopes [1–3]. More recently, nonlinear propagation and modal interaction has become very active towards rich nonlinear physics and multimode photonics devices [4–6].

One of the very interesting results of this recent revival of multimode nonlinear optics is that, when modal interaction and input power is significant enough, exchange of energy between the modes of an initially multi-modal beam can lead to a beam self-cleaning (BSC) into the lowest-order mode [7, 8]. This has spurred an interesting fundamental discussion regarding the nuances of the physical processes, and a number of further demonstrations where tuning the initial conditions can lead to BSC into specific higher-order modes [9–11].

Besides BSC, multimode interactions have been shown to tune supercontinuum generation [12–14], create interesting multimode soliton interactions [15–17], and even enable spatial-temporal mode-locking [18, 19] pushing toward enabled technologies. Beyond typical multimode fibers like the graded-index fibers used in most of the cited works, large diameter hollow-core fibers have also been a platform for multimode phenomena [20–22] pushing the frontier of short pulse duration and high pulse energy.

In our work we investigate beam self-cleaning, focusing on tuning the initial conditions to have the majority of the energy transfer to even higher-order modes than presented in past work. Specifically, we focus on tilt (propagation direction) and offset (central spatial position) of the input Gaussian beam, and their effects on the initial conditions at the fiber facet and on nonlinear propagation and BSC into higher-order modes. We focus on experimentally and theoretically simpler initial conditions than those of past work [10]. Finally, we discuss using relatively simple spatio-temporal initial conditions, where each mode has a different temporal profile, to further tune the BSC process.

2. Mode Coupling

Our work is purely numerical. The modeling of nonlinear multimode fiber propagation is a difficult general problem due to the complexity and/or resolution of the dynamics, and can be done in a number of ways [23–25] with different advantages. We use a technique based on a modal decomposition [26] that can be easily parallelized to speed up computation. Therefore we need to know the complex initial conditions in each mode before simulating the nonlinear propagation.

When a light pulse-beam is injected into a multimode fiber, its energy is distributed among the various propagating (spatial) modes based on the properties of the light beam at the input facet. Those modes for a graded-index fiber of 50 μm core diameter at 1064 nm central wavelength are shown in figure 1.a, where the ordering is according to the decreasing propagation constant in our case rather than the radial or rotational order of the mode. The energy distribution in each mode is described by the coupling coefficient [27–29]:

$$\eta_i = \frac{|\int \int p(x, y, \Delta z) F_i(x, y) dx dy|^2}{\int \int |p(x, y, \Delta z)|^2 dx dy \int \int |F_i(x, y)|^2 dx dy}, \quad (1)$$

where F_i represents the transverse profile of the mode, and p is the spatial profile of the injected pulse. This coupling coefficient quantifies the overlap between the beam and the mode of interest, with a unique coefficient for each mode. The method of injecting a light pulse into the fiber significantly influences the coupling coefficient, as it alters the overlap between the pulse and the different modes. Key parameters that affect this overlap include the transverse [14] and longitudinal [30] offsets, the beam waist (intensity half-width measured at $1/e^2$), and the tilt angle [9, 22] of the injected beam. In this analysis, a zero longitudinal offset is assumed, although in past work that has also shown to affect nonlinear processes [30]. It is important to note that these parameters represent experimental degrees of freedom, i.e. our aim is to work only with initial conditions that are relevant to simple and realistic experimental scenarios.

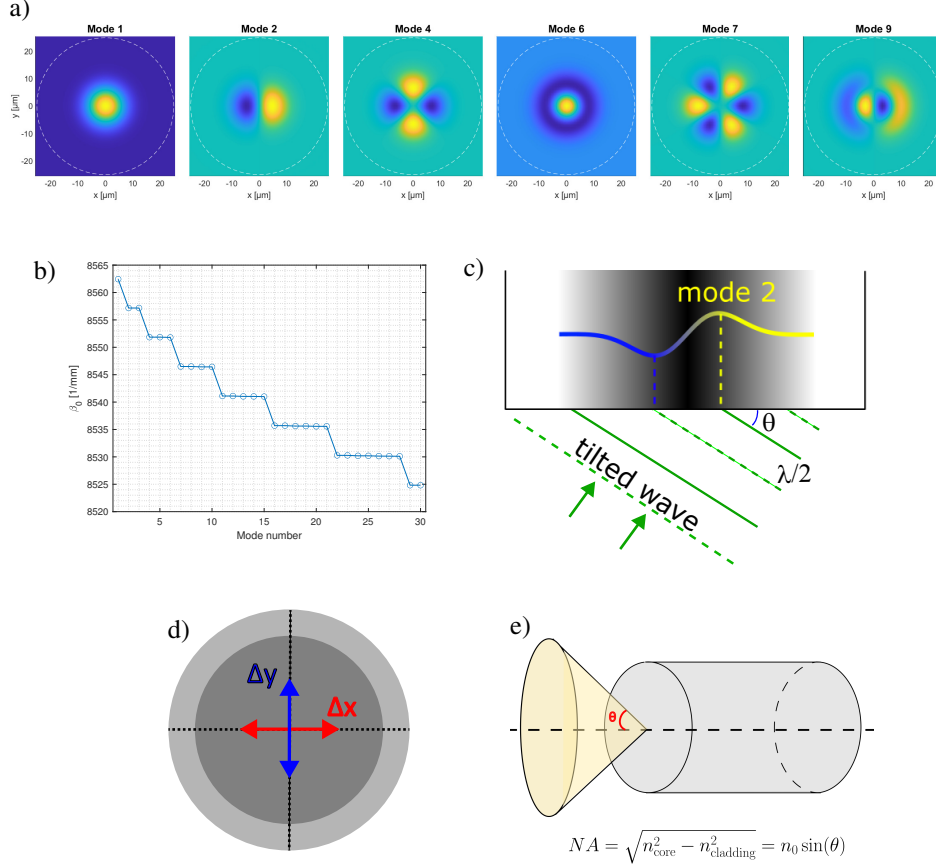


Fig. 1. a) Transverse profile of even modes in the y direction. The outline of the fiber core is shown in white dotted lines, the diameter is 50 μm . b) Propagation constants. c) Tilt angle ($\theta \in [0^\circ, 5^\circ]$). d) Offset in transverse directions ($\Delta x \in [0 \mu\text{m}, 15 \mu\text{m}]$). e) Numerical aperture ($NA = 0.2$) and its associated acceptance cone.

In the specific case of zero transverse offset and zero tilt angle (see figure 1), the energy of a Gaussian pulse is not coupled into modes that are antisymmetric in the x- or y-direction, as the overlap integral evaluates to zero. Under these conditions, only modes exhibiting cylindrical symmetry are excited (e.g., modes 1, 6, and 15 according to our numbering, presented in figure 1.a and 1.b). When a nonzero transverse offset is introduced (see figure 1.d), the symmetry is broken, resulting in nonzero coupling coefficients for antisymmetric modes. For instance, if there is a nonzero offset in the x-direction then even modes in the y-direction are excited (see figure 1.a) while odd modes in y-direction have still zero coupling.

The first panel of figure 2 illustrates that the energy coupled into the fundamental mode decreases as the offset increases. This occurs because the fundamental mode has a finite size. As the input pulse is injected with a greater offset, its overlap with the fundamental mode diminishes, ultimately resulting in an almost zero-coupling coefficient at an offset of 15 μm in the x-direction. Since each mode is centered within the fiber and the size of the mode increases with its order (see

figure 1.a), a larger transverse offset leads to the excitation of higher-order modes. Additionally, the total energy transmitted into the fiber decreases with increasing offset. This is mainly because, at a certain offset, there won't be any guided modes that overlap with the portion of the input beam the furthest from the fiber center, i.e. that portion is directly unguided and leaves the fiber.

The second row of figure 2 shows that as the waist of the injected beam increases, the guided energy decreases. The remaining energy is mostly redistributed among the cylindrical modes. This observation aligns with expectations since the impact of the offset becomes less significant for broader beams than for narrower ones. For a large beam waist, the symmetry-breaking effect of a nonzero offset becomes negligible, and only the overlap integrals of cylindrical modes yield significant values.

It is worth noting that the phase also plays a significant role in mode coupling, since the spatial function of the beam in Eq. 1 is complex and the mode profiles can have positive and negative regions. In the case of zero transverse offset but a nonzero tilt angle, see the third panel of figure 2, variations in the tilt angle modify the overlap between the Gaussian input pulse and the propagation modes (see figure 1.c). This change in overlap affects the energy distribution at the entry of the fiber. As the tilt angle of the injected pulse increases, higher-order modes become more sensitive to the matching of the spatial phase due to their larger transverse spatial extent. Additionally, there is less energy losses compared to the case of an increasing offset since the pulse is still centered. Still, at a high enough input tilt angle, fewer light rays will enter the acceptance cone of the fiber. This cone is directly related to the numerical aperture of the fiber, as shown in figure 1.e. In this simplified picture, light rays outside this cone fail to undergo total internal reflection and are therefore not guided. Note that the numerical aperture also determines the number of guided modes through the normalized frequency. In this paper, $NA = 0.2$ (index contrast 0.0137) meaning that roughly 218 modes are guided.

For a fixed tilt angle, increasing the beam waist shifts the energy distribution toward higher-order modes, as illustrated in the fourth panel of figure 2. This effect occurs mainly because higher-order modes are larger, and a broader input pulse enhances the corresponding overlap integrals.

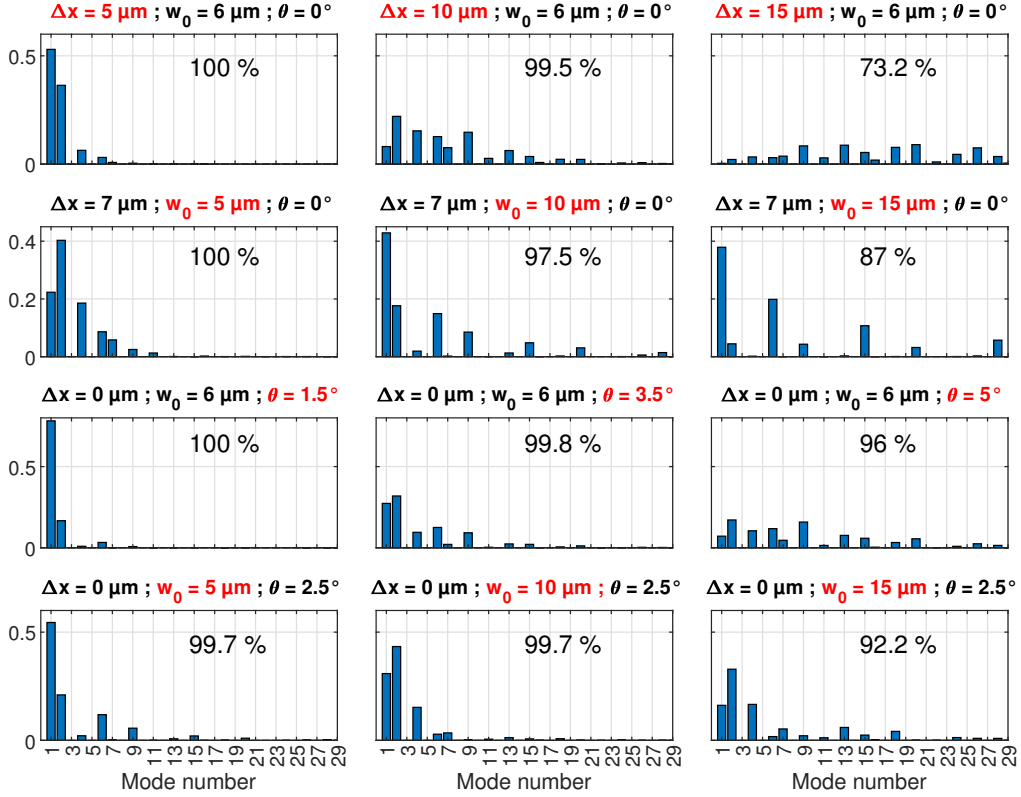


Fig. 2. Energy distribution into the propagation modes of the fiber at its entry. For each panel of the figure a different parameter was modified. The modified parameters are (from top to bottom): Offset in x-direction (Δx), waist (w_0) at a fixed offset, tilt angle (θ), and again waist but at a fixed tilt angle. The percentage in each panel gives the fraction of the energy that is guided in that case.

3. Beam self-cleaning

In the previous section, we demonstrated that the energy distribution at the entry of the fiber can be altered by adjusting the waist and offset of the input pulse. By influencing this initial energy distribution among the propagation modes, it is possible to affect the interactions between these modes during propagation, which occur due to nonlinear processes.

This paper focuses on a specific nonlinear phenomenon unique to multimode fibers, known as beam self-cleaning. Beam self-cleaning involves a redistribution of energy among the modes during propagation, driven by intermodal four-wave mixing (IFWM). This process results in a net transfer of energy towards a single dominant mode, causing the transverse profile of the pulse within the fiber to resemble that of the dominant mode. Beam self-cleaning can thus be interpreted as a restructuring of the transverse profile of the pulse during propagation. While the most common beam self-cleaning outcome is a transfer into the fundamental mode, it has also been shown that beam self-cleaning into mode 2 is possible with simple initial conditions [9, 11], and higher modes too with more complex wavefront tuning [10].

In this section, we investigate how the offset and tilt angle of the input pulse influence beam self-cleaning. The simulations presented here consider a fiber with a core diameter of $50 \mu\text{m}$, a numerical aperture $NA = 0.2$, and a nonlinear refractive index $n_2 = 3.2 \times 10^{-20} \text{ V}^{-2} \text{ m}^2$. The fiber length is 30 cm (with the exception of subsection 3.2). The injected pulse is a Gaussian beam of central wavelength 1064 nm with a full width at half maximum duration of 90 fs and containing an energy of 38 nJ, emulating the parameters in Ref. [7].

3.1. Beam self-cleaning into mode 2

By varying the offset and the waist, we can observe that figure 3 highlights the specific case where mode 2 receives the most energy during propagation. This beam self-cleaning into mode 2 was achieved by considering a waist of $6\ \mu\text{m}$ and an offset of $7\ \mu\text{m}$. However, the optimal offset value actually does not correspond to the position of the maximum amplitude of mode 2. One might expect that aiming the input beam at the maximum of one of the lobes of mode 2 would maximize energy coupling into this mode. In reality, the offset value that provides the greatest energy gain for mode 2 is higher. This is due to the overlap with the fundamental mode. Indeed, when the input beam is directed toward one of the lobes of mode 2, the Gaussian beam, being larger than the lobe, does not achieve perfect overlap, resulting in a coupling coefficient less than one. Consequently, the remaining energy is distributed among other modes. Since the overlap integral with the fundamental mode is greater than that with mode 2, a significant portion of the energy is coupled into the fundamental mode instead of mode 2.

On the left side of figure 3, the energy distribution at the entry of the fiber is depicted. Utilizing a small but nonzero offset results in the energy being primarily distributed among lower-order modes. Specifically, approximately 80 % of the input energy is distributed into modes 1, 2, and 4 (see figure 1.a). These modes, which account for the majority of the energy coupled into the fiber, are also the most likely to interact with one another, as their propagation constants are similar (see figure 1.b), resulting in small phase detuning. This enables energy exchange through intermodal four-wave mixing over a relatively long distance, leading to a net transfer of energy to mode 2, as shown in the right image of figure 3. The outcome is a reshaping, or cleaning, of the transverse profile, revealing the mode 2 profile.

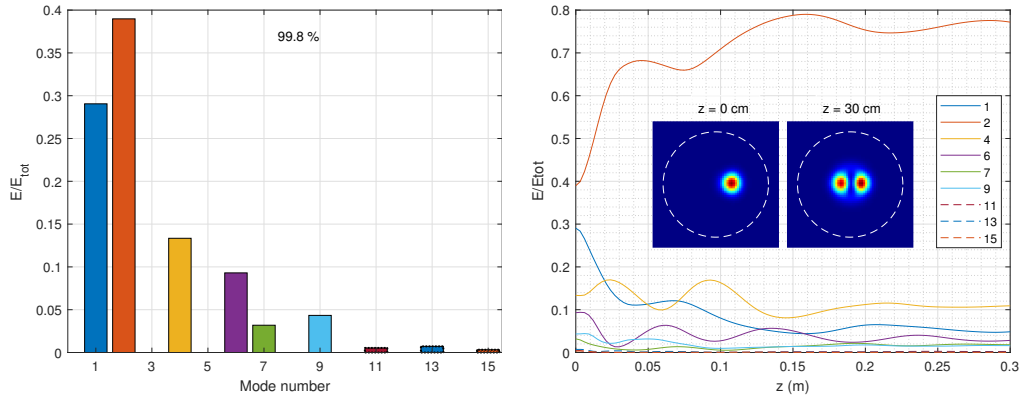


Fig. 3. On the left : Initial energy distribution into a basis of 15 propagating modes after injecting a Gaussian pulse with a $7\ \mu\text{m}$ horizontal offset. The percentage gives the fraction of the energy that is guided by these modes. On the right : Evolution of normalized modal energies versus propagation distance and transverse intensity profile of the pulse at the entry of the fiber (leftmost profile) and after 30 cm of propagation (rightmost profile). The outline of the fiber core is shown in white dotted lines.

In a case where a Gaussian pulse with a waist of $10\ \mu\text{m}$ and a tilt angle of 2.5° (and no offset) is injected into the fiber, the energy distribution is relatively similar to the case with an offset, though 98.5 % of the energy is coupled into the 15 modes compared to 99.8 % for the case with a nonzero offset. This energy distribution still results in beam self-cleaning into mode 2, achieving nearly the same fraction of the total energy after 30 cm of propagation as in the offset case, though with greater injection losses.

The evolution of the transverse profile during propagation leads to a reshaping of the initial Gaussian profile into the transverse profile of mode 2. While the profile at the entry of the fiber is not perfectly Gaussian, increasing the number of modes improves its reconstruction. This suggests that the 15-mode approximation, while computationally efficient, may not fully capture the complexity of the initial field distribution.

When increasing the number of modes to 20, the initial transverse profile more closely resembles a Gaussian, as shown in the leftmost profile of figure 4. Additionally, increasing the number of modes enhances energy coupling efficiency at injection since higher-order modes, such as mode 18, now capture a portion of the energy that would otherwise be lost. Despite these refinements, the overall energy redistribution during propagation, primarily governed by intermodal four-wave mixing, remains consistent between the two cases. After 30 cm of propagation, the energy in mode 2 differs by only 2.5 % between the 15- and 20-mode scenarios. This small difference suggests that beyond a certain point, increasing the number of modes yields only marginal improvements in accuracy while significantly increasing computational costs.

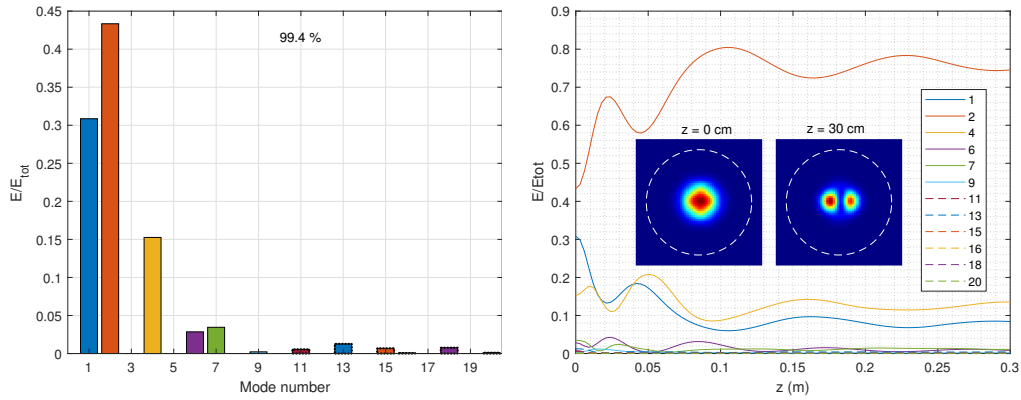


Fig. 4. On the left : Initial energy distribution into 20 propagation modes after injecting a tilted Gaussian pulse. The percentage gives the fraction of the energy that is contained in those 20 modes. On the right : Evolution of normalized modal energies versus propagation distance and transverse intensity profile of the pulse at the entry of the fiber (leftmost profile) and after 30 cm of propagation (rightmost profile). The outline of the fiber core is shown in white dotted lines.

For the previous case (see figure 3), increasing the number of modes from 15 to 20 has a negligible impact on the results. In the 20-mode case, 100 % of the energy is coupled into the fiber, compared to 99.8 % in the 15-mode case. The additional 0.2 % is distributed among high-order modes, such as modes 16 and 18, and has a negligible impact on the nonlinear phenomena occurring during propagation. Even when considering only 10 modes, the results remain satisfactory, as the energy in mode 2 after 30 cm of propagation differs by only 7 %. This demonstrates that even a reduced number of modes can provide meaningful insights while significantly lowering computational costs.

In conclusion, when a pulse is injected with a nonzero tilt angle, more modes are excited compared to the no-tilt case. Consequently, the number of modes considered in the simulation should be adjusted to account for these additional contributions.

3.1.1. Discussion about beam self-cleaning into mode 2

Figures 3 and 4 show that the transverse profile of the pulse-beam can be reshaped into the transverse profile of mode 2. It is also worth noting that the remaining modes retain a small

fraction of their energy, contributing to an increase of the entropy of the overall system. For instance, in the case of figure 3, the remaining modes (modes 1, 4, 6, 7, and 9) collectively retain approximately 22 % of the initial energy. These modes form a noisy background upon which the transverse profile of mode 2 emerges. This background noise is not a problem, because what is of interest here for applications is beam intensity. Since the intensity of the lobes is much greater than that of the noise, nonlinear effects will only occur in the spatial region occupied by the lobes with the greatest intensity.

These high-intensity lobes can be thought of as nonlinear waveguides, since they locally increase the value of the refractive index. The quality of these waveguides depends directly on the evolution of modal energies. In the case of figure 3, by inspecting the transverse profile at different points of propagation, we see that energy is well distributed in both lobes leading to two optical waveguides. On the other hand, in the case of figure 4, the energy tends to be more distributed into one lobe so only one optical waveguide can be considered. This is still interesting since a lobe of mode 2 is smaller than the lobe of the fundamental mode.

3.2. Beam self-cleaning into mode 4

In this subsection, we demonstrate that by using a larger offset, higher-order modes can be excited, leading to beam self-cleaning into a mode previously inaccessible with such simple initial conditions. By using a waist of 6 μm and an offset of 10 μm , beam self-cleaning into mode 4 can be achieved, as shown in the figure 5. The left panel of this figure illustrates the energy distribution at the fiber entry. In this subsection, a fiber length of 50 cm is considered. A larger offset than in the previous subsection is used because the lobes of mode 4 are located farther from the fiber center than those of mode 2. As before, targeting a lobe of mode 4 with the input pulse requires an offset greater than the position of the maximum of the lobe. This is due to the influence of the fundamental mode as well as mode 2.

For the simulation, 20 modes were considered because injecting the Gaussian pulse with a higher offset excites a larger number of modes. It is therefore necessary to include enough modes to ensure that the energy distribution is accurately represented. A simulation with 25 modes was also performed, but no significant differences were observed compared to the 20-mode case, indicating that the latter is a reasonable approximation. In the 25-mode simulation, 98.6 % of the energy was injected into the multimode fiber, compared to 97.9 % for the 20-mode case. The 0.7 % difference was distributed between modes 22 and 24, which carry too little energy to significantly impact the results. Consequently, these higher-order modes can be neglected without compromising the accuracy of the simulation.

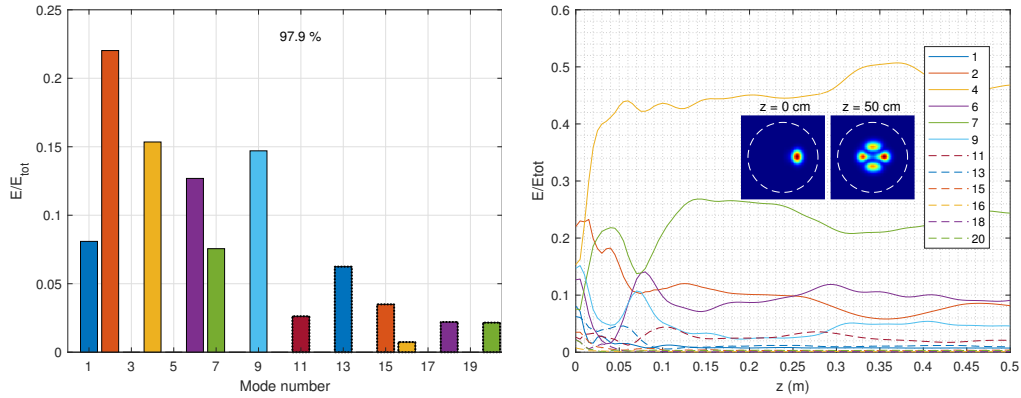


Fig. 5. On the left : Initial energy distribution into 20 propagation modes after injecting a Gaussian beam with a $10 \mu\text{m}$ horizontal offset. The percentage gives the fraction of the energy that is guided in those 20 modes. On the right : Evolution of normalized modal energies versus propagation distance and transverse intensity profile of the pulse at the entry of the fiber (leftmost profile) and after 50 cm of propagation (rightmost profile). The outline of the fiber core is shown in white dotted lines.

The left panel shows that, for this offset, the energy is primarily distributed among modes 2 through 9 (see figure 1.a for mode numbering). During propagation, modes 4 and 7 gain energy via inter-modal four-wave mixing. Mode 4 quickly becomes the dominant mode, although mode 2 initially carried the most energy. Consequently, the transverse profile of the pulse-beam is reshaped to match that of mode 4. However, mode 7 retains approximately 24 % of the initial energy, which leads to fluctuations in the transverse profile during propagation due to interference between modes 4 and 7.

3.2.1. Discussion about beam self-cleaning into mode 4

The figure 5 shows the transverse profile of the pulse at the output of the fiber. During propagation, the transverse profile was restructured from a single Gaussian lobe into four distinct lobes. However, when compared with the transverse profile of mode 4 shown in figure 1, it becomes evident that, while the four lobes are separated, they are also distorted due to interference with mode 7. To achieve improved beam self-cleaning, mode 7 would need to transfer its energy to mode 4. In such a case, the transverse profile would experience significantly fewer fluctuations during propagation through the multimode fiber and lobes would be more symmetric. In the case illustrated in the figure 5, two of the lobes exhibit sufficiently high intensity to function as nonlinear optical waveguides, for example.

3.3. Beam self-cleaning into mode 7

As in the previous subsection, we demonstrate here that varying one of the injection parameters allows for the observation of a beam self-cleaning into a new higher-order mode, not previously accessible with these simple initial conditions. As shown in figure 6, injecting a Gaussian tilted pulse-beam with a waist of $10 \mu\text{m}$ and a tilt angle of 5° (see figure 1.c) results in beam self-cleaning into mode 7. In this case, most of the energy at the fiber entry is distributed among modes 4 through 13, with mode 9 being the dominant mode initially. By comparing the left panels of the figures 4 and 6, it is evident that increasing the tilt angle leads to the excitation of a significantly larger number of modes (for a fixed waist), as mentioned in section 2. This implies that the number of modes considered in simulations must increase with the tilt angle. We

can see that the transverse profile of the pulse at the very beginning of the fiber does not look like a perfect bell shape. Increasing the number of modes to be considered in the basis to 30 improves the transverse profile, but new modes contains less than 1% of the total energy so they are negligible in the propagation simulation. Furthermore, increasing the waist results in more energy being coupled into higher-order modes, as shown in the fourth panel of figure 2.

Note that it is also possible to obtain beam self-cleaning into mode 7 by using no tilt, but a small waist (e.g. $6\ \mu\text{m}$) with a large transverse offset (e.g. $13\ \mu\text{m}$). Nevertheless, in such a case, mode 7 gains generally less energy than in a case with nonzero tilt. It is also important to note that the method used to aim at a lobe of the mode of interest is not efficient for mode 7. This inefficiency arises because the lobes of mode 7 are relatively small and located far from the center of the fiber. Additionally, the influence of lower-order modes must be taken into account when targeting one of the lobes of mode 7. This requires considering a higher offset than the position of the lobes themselves, as explained in subsection 3.1. However, this approach necessitates using a very small waist and a large offset, which are not realistic experimentally. A large offset leads to significant losses, while an extremely small waist is impractical to achieve in an experimental setup.

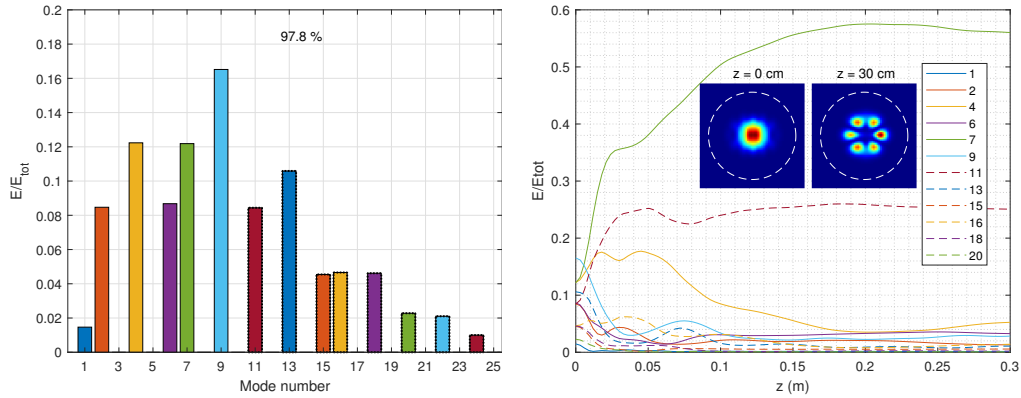


Fig. 6. On the left : Initial energy distribution into 25 propagation modes after injecting a Gaussian beam with a 5° tilt angle. The percentage gives the fraction of the energy that is guided in those 25 modes. On the right : Evolution of normalized modal energies versus propagation distance and transverse intensity profile of the pulse at the entry of the fiber (leftmost profile) and after 30 cm of propagation (rightmost profile). The outline of the fiber core is shown in white dotted lines.

As shown in figure 6, a net transfer of energy occurs during propagation, primarily toward modes 7 and 11. Mode 7 rapidly becomes the dominant mode, while the energy in mode 11 saturates earlier than in mode 7. Consequently, the transverse profile of the Gaussian beam is reshaped to match that of mode 7. Mode 11, carrying approximately 25 % of the incident pulse energy, has enough energy compared to mode 7 to create significant interference with it. This interference results in a transverse profile that may fluctuate during propagation.

3.3.1. Discussion about beam self-cleaning into mode 7

As described before, the transverse profile of mode 7 emerges during propagation. Specifically, the Gaussian lobe at the fiber entry is subdivided into six (nearly) distinct lobes that characterize the transverse profile of mode 7. However, when compared to the transverse profile of mode 7 shown in figure 1, we see that the lobes are slightly deformed, and some are not entirely

separated from their neighbors. This deformation arises from interference caused by higher-order modes—in this case, mode 11—which carries enough energy to alter the lobes.

In an ideal scenario, mode 11 would transfer part of its energy to mode 7, eventually reaching the same low energy level as the other higher-order modes. In such a case, the transverse profile would remain more stable throughout propagation. The influence of higher-order modes would be minimized, resulting in well-separated and symmetrical lobes that are free from deformation. Lobes that are stable through propagation could be used as nonlinear optical waveguides.

4. Spatial chirp

In this section, we consider an input light pulse-beam that is space-time coupled, meaning that the spatial and temporal variables in the equation characterizing the pulse are not separable [31]. Physically, this coupling leads to a distinct spatial behavior for each frequency component of the pulse. In other words, when the pulse is injected into the multimode fiber, each frequency component enters with different initial conditions. This phenomenon is not accounted for by the coupling coefficient presented in Eq. (1), necessitating the use of the following coupling coefficient [29]:

$$\mu_i(\omega) = \frac{\int \int \tilde{A}(x, y, \Delta z, \omega) F_i(x, y) dx dy}{\sqrt{\int \int |\tilde{A}(x, y, \Delta z, \omega)|^2 dx dy \int \int |F_i(x, y)|^2 dx dy}}. \quad (2)$$

This coefficient, which measures the coupling of the input field into each mode, is a frequency-dependent complex number. Consequently, μ_i represents a complex frequency envelope rather than an efficiency, as η_i does. The coupling efficiency into mode i is given by $\int |\mu_i(\omega)|^2 d\omega$.

In this paper, the space-time coupling studied is the so-called spatial chirp. In this case, each frequency component of the pulse has a different transverse offset at the focus point of the beam. In the time domain, spatial chirp corresponds to focusing a tilted pulse front. The frequency distribution along the transverse direction is described by $x_0(\omega) = w_0 \tau_t \delta\omega / 2$, where w_0 is the beam waist, $\delta\omega$ is the frequency offset relative to the central frequency of the pulse, and τ_t is the amount of pulse-front tilt applied to the collimated beam to generate spatial chirp in the focused beam.

In the following analysis, we consider the injection of a Gaussian pulse-beam with a waist of 4 μm and a transverse offset in the x -direction of 5 μm . In one scenario, there is no spatial chirp ($\tau_t = 0$), while in the other, $\tau_t = \tau_0$, where $\tau_0 = \text{FWHM} / \sqrt{2 \ln(2)}$. Figure 7 shows energy distribution among modes at the beginning of the multimode fiber in a case without spatial chirp (figure 7.a) and in a case with spatial chirp (figure 7.b). It also shows the evolution of modal energies for the case without spatial chirp (figure 7.c) and the case with it (figure 7.d). In both cases, we have a beam self-cleaning into mode 2.

First, spatial chirp impacts the energy distribution among modes but it also changes the spectrum of each mode individually, as shown in the figure 7.a and 7.b, leading to a new degree of freedom to impact nonlinear interactions between modes during propagation. In the case with spatial chirp, the fundamental mode initially carries more energy than mode 2. Additionally, 98.7% of the total energy is coupled into the 15 modes of the multimode fiber that we consider, which is slightly less than in the case without spatial chirp. By the end of propagation, mode 2 retains less energy than in the case without spatial chirp, but it also begins propagation with a lower initial energy.

Furthermore, in the presence of spatial chirp, the energy of mode 2 fluctuates significantly less during propagation. This change in modal energy evolution arises because the modes have different spectra at the input of the fiber (see figure 8.a and 8.d), altering the nonlinear interactions between modes that govern their energy exchange.

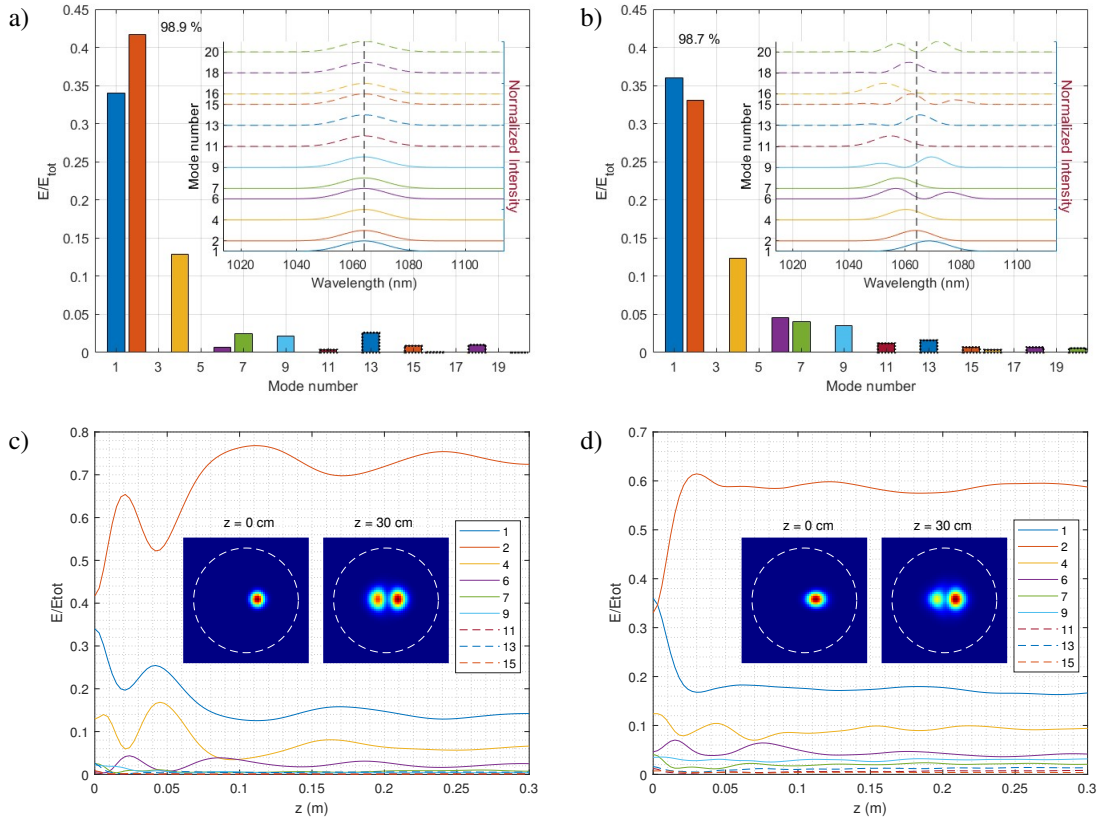


Fig. 7. a) Energy distribution among 15 modes at the entry of the multimode fiber and spectra of the excited modes in a case without spatial chirp. The black vertical line indicates the central wavelength of the input pulse. b) Energy distribution among 15 modes at the entry of the multimode fiber and spectra of the excited modes in a case with spatial chirp. The black vertical line indicates the central wavelength of the input pulse. c) d) In a case without and with spatial chirp respectively : Evolution of normalized modal energies versus propagation distance and transverse intensity profile of the pulse-beam. The outline of the fiber core is shown in white dotted lines.

In the case of a positive spatial chirp combined with a positive transverse offset, longer wavelengths are more eccentric than shorter wavelengths. Consequently, the higher the mode order, the more its spectrum is centered at longer wavelengths. Figure 8 presents spectrograms of modes 1 and 2 at different points along the fiber. At the beginning of propagation, the spectra of the modes are slightly offset from the central frequency of the incident pulse (1064 nm). The spectrum of mode 2 is slightly shifted toward longer wavelengths (see figure 8.b), while the spectrum of the fundamental mode is shifted toward shorter wavelengths (see figure 8.a). Higher-order modes generally exhibit spectra shifted toward longer wavelengths. This spectral shift also affects the temporal shapes of the modes, making them temporally broader compared to the case without spatial chirp. After 5.1 cm of propagation (see figures 8.b and 8.e), the spectrum of the fundamental mode broadens and shifts to shorter wavelengths, with most of its spectrum lying between 1016 nm and 1090 nm. The spectrum of mode 2, on the other hand, splits into two distinct lobes: a primary lobe at approximately 1121 nm and a secondary lobe at around 1010 nm. While some frequencies exist between these lobes, they constitute only a minor part of the spectrum.

At the end of the fiber (see figures 8.c and 8.f), the spectrum of the fundamental mode consists of a primary lobe centered around 1016 nm, followed by a tail extending from 1032 nm to 1088 nm. In contrast, the spectrum of mode 2 shifts further toward longer wavelengths, spanning primarily between 1020 nm and 1062 nm, with a small lobe centered around 989 nm.

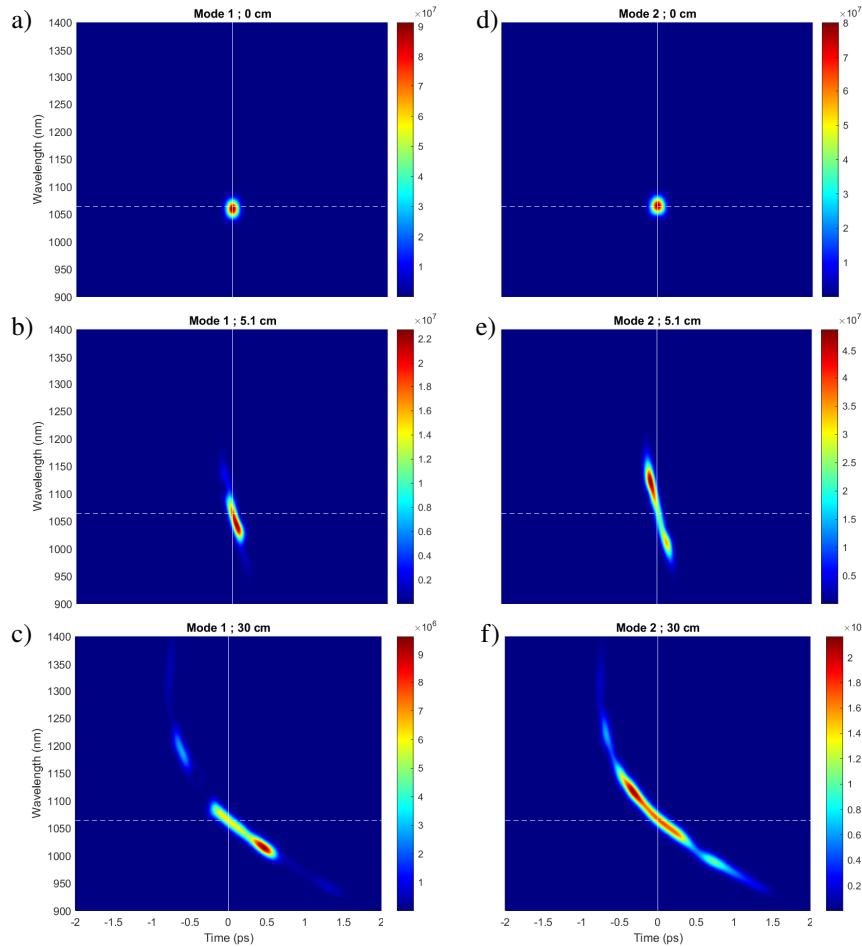


Fig. 8. a) b) c) Spectrograms of mode 1 after 0 cm, 5.1 cm and 30 cm of propagation, respectively. d) e) f) Spectrograms of mode 2 after 0 cm, 5.1 cm and 30 cm of propagation, respectively. The white dotted line indicates the central wavelength of the input pulse. The white vertical line indicates time zero.

4.1. Discussion

The difference in modal energy evolution between cases with and without spatial chirp arises from the distinct evolution of the mode spectra. In the case without spatial chirp, the fundamental mode and mode 2 exhibit a similar spectral evolution during the first centimeters of propagation. Because they share comparable frequency components, they propagate at nearly the same speed and they have a small phase mismatch that facilitates significant energy exchange through inter-modal four-wave mixing.

However, this behavior changes in the presence of spatial chirp. Figures 8.b and 8.e show that after 5.1 cm of propagation, the spectra of modes 1 and 2 have different shapes, sharing fewer overlapping points on the time grid. At 5.1 cm, the bulk of the fundamental mode spectrum no

longer coincides temporally with the spectrum of mode 2. The latter is now primarily composed of two lobes: one at a lower frequency than the fundamental mode spectrum and the other at a higher frequency. Due to chromatic dispersion, these lobes propagate at different speeds, leading to a temporal separation (imperfect overlap) between the fundamental mode and mode 2. This separation prevents the two modes from exchanging energy via inter-modal four-wave mixing after this point, since it is an instantaneous nonlinear process. Moreover, as the spectra of the modes increasingly differ in frequency content, the phase mismatch grows, further reducing the potential for energy exchange. The small fluctuations observed during propagation are due to the modes maintaining limited spectral overlap. As shown in the figure 8.c, the tail of the fundamental mode spectrum shares certain wavelengths with mode 2, allowing for minor energy exchange.

In sum, the above phenomena cause the evolution of the exchange of energy between mode 1 and mode 2 to essentially finish after a shorter propagation distance in the fiber when spatial chirp is present. The oscillations in the energy of mode 2, which characterize an exchange of energy (beating) between mode 1 and mode 2, are no longer as strong. Such a control is enabled by the spatial chirp and is not necessarily possible by controlling another parameter such as initial energy.

5. Conclusion

In conclusion, we conducted a numerical study on the impact of initial conditions on the nonlinear interactions occurring during the propagation of a femtosecond optical pulse in a multimode fiber. By varying the transverse offset, waist, and tilt angle of the input Gaussian pulse-beam, we demonstrated that the energy distribution among the modes of the fiber can be effectively controlled.

We numerically showed that by adjusting the injection parameters of the Gaussian pulse-beam, beam self-cleaning can be achieved in higher-order modes such as modes 2, 4, and 7. The higher the order of the targeted mode, the more difficult it is to achieve such a cleaning—in terms of the extremity of the initial conditions necessary and the competition with other modes upon propagation. Additionally, we examined the influence of the number of modes considered in the simulations, highlighting the trade-off between accuracy and computational efficiency.

Furthermore, we demonstrated that considering an input pulse with space-time coupling provides an additional degree of freedom for controlling nonlinear propagation, as each mode exhibits distinct temporal profiles. Specifically, we considered spatial chirp which induces at the focal point of the beam a spatial transverse separation of the frequency components of the input pulse. With such a space-time coupling, we showed numerically that it can be used to tune beam self-cleaning by altering spectral evolution during propagation. Specifically, we showed that the spatial chirp could stabilize the beam cleaning at a shorter propagation distance while only mildly reducing the quality of said cleaning. Our findings open new avenues for the controlled manipulation of nonlinear dynamics in multimode fibers by leveraging a high-dimensional space of initial conditions.

Funding. Fonds De La Recherche Scientifique - FNRS.

Disclosures. The authors declare no conflicts of interest.

Data Availability Statement. Data underlying the results presented in this paper are not publicly available at this time but may be obtained from the authors upon reasonable request.

References

1. T. Čižmár and K. Dolakia, "Exploiting multimode waveguides for pure fibre-based imaging," *Nat. Commun.* **3**, 1027 (2012).
2. M. Plöschner, T. Tyc, and T. Čižmár, "Seeing through chaos in multimode fibres," *Nat. Photonics* **9**, 529–535 (2015).

3. H. Cao, T. Čižmár, S. Turtaev, *et al.*, “Controlling light propagation in multimode fibers for imaging, spectroscopy, and beyond,” *Adv. Opt. Photonics* **15**, 524–612 (2023).
4. K. Krupa, A. Tonello, A. Barthélémy, *et al.*, “Multimode nonlinear fiber optics, a spatiotemporal avenue,” *APL Photonics* **4**, 110901 (2019).
5. L. G. Wright, W. H. Renninger, D. N. Christodoulides, and F. W. Wise, “Nonlinear multimode photonics: nonlinear optics with many degrees of freedom,” *Optica* **9**, 824–841 (2022).
6. L. G. Wright, F. O. Wu, D. N. Christodoulides, and F. W. Wise, “Physics of highly multimode nonlinear optical systems,” *Nat. Phys.* **18**, 1018–1030 (2022).
7. Z. Liu, L. G. Wright, D. N. Christodoulides, and F. W. Wise, “Kerr self-cleaning of femtosecond-pulsed beams in graded-index multimode fiber,” *Opt. Lett.* **41**, 3675–3678 (2016).
8. K. Krupa, A. Tonello, B. M. Shalaby, *et al.*, “Spatial beam self-cleaning in multimode fibres,” *Nat. Photonics* **11**, 237–242 (2017).
9. E. Deliancourt, M. Fabert, A. Tonello, *et al.*, “Kerr beam self-cleaning on the lp11 mode in graded-index multimode fibers,” *OSA Continuum* **2**, 1089–1096 (2019).
10. E. Deliancourt, M. Fabert, A. Tonello, *et al.*, “Wavefront shaping for optimized many-mode kerr beam self-cleaning in graded-index multimode fiber,” *Opt. Express* **27**, 17311–17321 (2019).
11. J. Chen, W. Hong, and A. Luo, “Nonlinear dynamics of beam self-cleaning on LP11 mode in multimode fibers,” *Opt. Express* **30**, 43453–43463 (2022).
12. L. G. Wright, D. N. Christodoulides, and F. W. Wise, “Controllable spatiotemporal nonlinear effects in multimode fibres,” *Nat. Photonics* **9**, 306–310 (2015).
13. L. G. Wright, S. Wabnitz, D. N. Christodoulides, and F. W. Wise, “Ultrabroadband dispersive radiation by spatiotemporal oscillation of multimode waves,” *Phys. Rev. Lett.* **115**, 223902 (2015).
14. M. A. Eftekhar, L. G. Wright, M. S. Mills, *et al.*, “Versatile supercontinuum generation in parabolic multimode optical fibers,” *Opt. Express* **25**, 9078–9087 (2017).
15. L. G. Wright, W. H. Rinneinger, D. N. Christodoulides, and F. W. Wise, “Spatiotemporal dynamics of multimode optical solitons,” *Opt. Express* **23**, 3492–3506 (2015).
16. Y. Sun, M. Zitelli, M. Ferraro, *et al.*, “Multimode soliton collisions in graded-index optical fibers,” *Opt. Express* **30**, 21710–21724 (2022).
17. Y. Sun, P. Parra-Rivas, G. P. Agrawal, *et al.*, “Multimode solitons in optical fibers: a review,” *Photonics Res.* **12**, 2581–2632 (2024).
18. L. G. Wright, D. N. Christodoulides, and F. W. Wise, “Spatiotemporal mode-locking in multimode fiber lasers,” *Science* **358**, 94–97 (2017).
19. L. G. Wright, P. Sidorenko, H. Pourbeyram, *et al.*, “Mechanisms of spatiotemporal mode-locking,” *Nat. Phys.* **16**, 565–570 (2020).
20. R. Safaei, G. Fan, O. Kwon, *et al.*, “High-energy multidimensional solitary states in hollow-core fibres,” *Nat. Photonics* **14**, 733–739 (2020).
21. R. Piccoli, J. M. Brown, Y.-G. Jeong, *et al.*, “Intense few-cycle visible pulses directly generated via nonlinear fibre mode mixing,” *Nat. Photonics* **15**, 884–889 (2021).
22. C. Brahm and J. C. Travers, “Soliton self-compression and resonant dispersive wave emission in higher-order modes of a hollow capillary fibre,” *J. Physics: Photonics* **4**, 034002 (2022).
23. F. Poletti and P. Horak, “Description of ultrashort pulse propagation in multimode optical fibers,” *J. Opt. Soc. Am. B* **25**, 1645–1654 (2008).
24. F. Tani, J. C. Travers, and P. S. Russell, “Multimode ultrafast nonlinear optics in optical waveguides: numerical modeling and experiments in kagomé photonic-crystal fiber,” *J. Opt. Soc. Am. B* **31**, 311–320 (2014).
25. P. Béjot, “Multimodal unidirectional pulse propagation equation,” *Phys. Rev. E* **99**, 032217 (2019).
26. L. G. Wright, Z. M. Ziegler, P. M. Lushnikov, *et al.*, “Multimode nonlinear fiber optics: Massively parallel numerical solver, tutorial, and outlook,” *IEEE J. Sel. Top. Quantum Electron.* **24**, 5100516 (2018).
27. J. Niu and J. Xu, “Coupling efficiency of laser beam to multimode fiber,” *Opt. Commun.* **274**, 315–319 (2007).
28. Z. Guang and Y. Zhang, “Coupling ultrafast laser pulses into few-mode optical fibers: a numerical study of the spatiotemporal field coupling efficiency,” *Appl. Opt.* **57**, 9835–9844 (2018).
29. S. W. Jolly and P. Kockaert, “Coupling to multi-mode waveguides with space-time shaped free-space pulses,” *J. Opt.* **25**, 054002 (2023).
30. A. S. Ahsan and G. P. Agrawal, “Effect of an input beam’s shape and curvature on the nonlinear effects in graded-index fibers,” *J. Opt. Soc. Am. B* **37**, 858–867 (2020).
31. S. Akturk, X. Gu, P. Bowlan, and R. Trebino, “Spatio-temporal couplings in ultrashort laser pulses,” *J. Opt.* **12**, 093001 (2010).